Thermal Quench, Current Quench, and Wall Forces in 3D VDE Computations with NIMROD

Carl Sovinec and Kyle Bunkers
University of Wisconsin-Madison

Theory and Simulation of Disruptions Workshop

July 16-18, 2018 Princeton, New Jersey

Center for Tokamak Transient Simulation

Outline

- Brief introduction
- General asymmetric VDE behavior
- MHD of current spike
- Computation of wall force
- Boundary modeling
- Conclusions & Discussion

Introduction

- Visco-resistive MHD NIMROD computations are being applied to understand asymmetric VDE physics.
  - Thermal quench
  - Current spike
  - Current quench
  - Wall forcing
- Problem parameters are those previously described.
  - $\tau_A \sim 1 \quad << \quad \tau_{\text{wall}} \sim 10^3 \quad << \quad \tau_\eta \sim 10^6$
  - $\chi_{||} = 10^4 \chi_\perp \quad ; \quad \nu_{||} = 10^3 \nu_\perp \quad ; \quad \text{Pm}(0) = 50$
- Better numerical resolution justifies detailed analysis.
  - $0 \le n \le 21$
  - Some cases have been evolved through CQ.

The 3D computations described here starts from an up-down symmetric equilibrium.

- $\beta(0) \cong 1\%$
- $q(0) = 1.75$

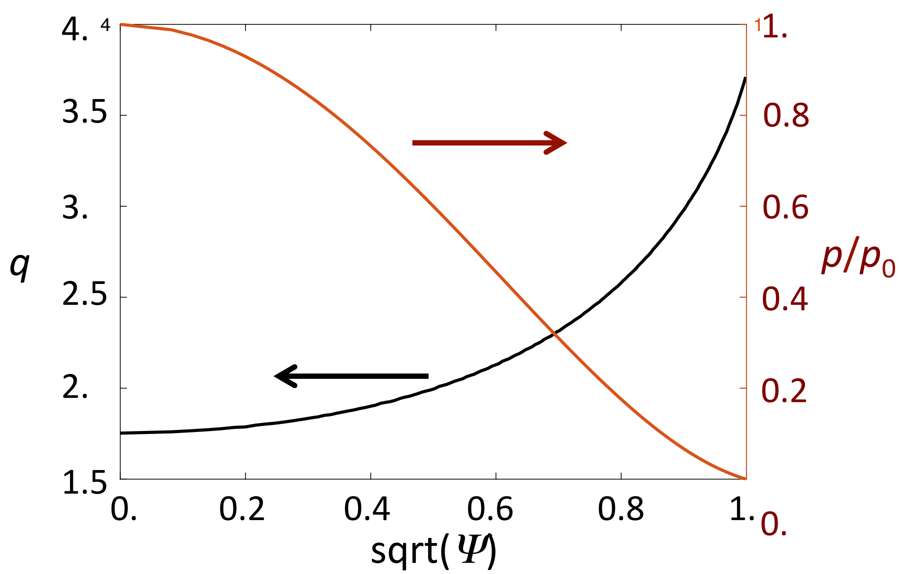

Safety factor and pressure profiles.

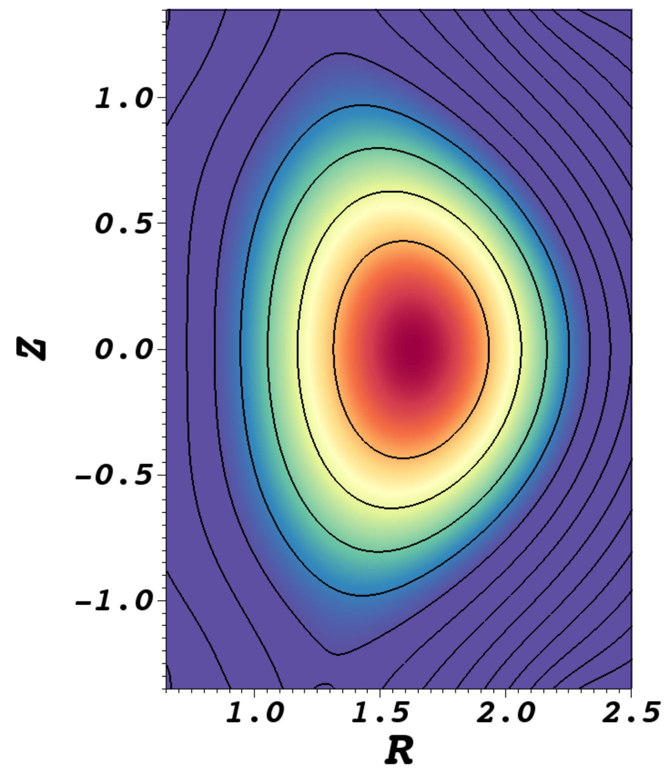

Contours of poloidal flux and pressure for the initial state. Border is the resistive wall.

- VDEs are initiated by removing current from the upper divertor coil (outside the resistive wall).

The edge of the initial profile is linearly unstable with a conducting wall.

- With the large edge resistivity and no flow, edge modes are unstable.

Growth rates computed for the initial equilibrium with conducting wall.

n	$\gamma\tau_A$
1	1.7×10^{-2}
2	-
3	1.8×10^{-3}
4	-

- Low-n growth rates increase only somewhat with a resistive wall with $\eta_{wall}/\mu_0\Delta x = 1\times10^{-3}$.

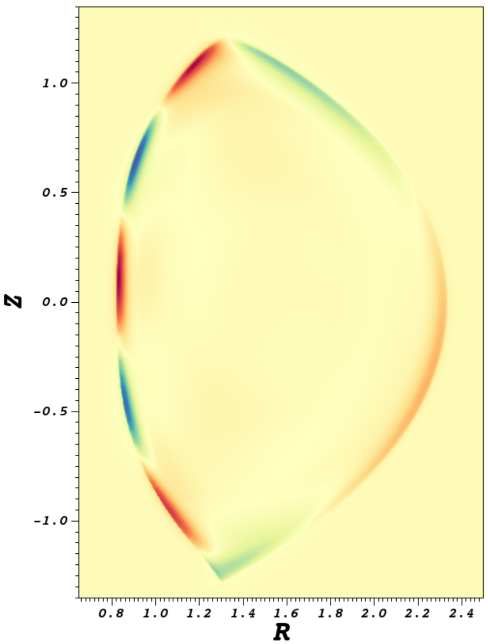

Peeling-type m = 4, n =1 mode is concentrated on the inboard side. (n = 1 pressure is shown.)

General behavior: Continuous MHD activity develops and evolves throughout the simulated transient.

- The dominant mode changes with increasing wall contact.

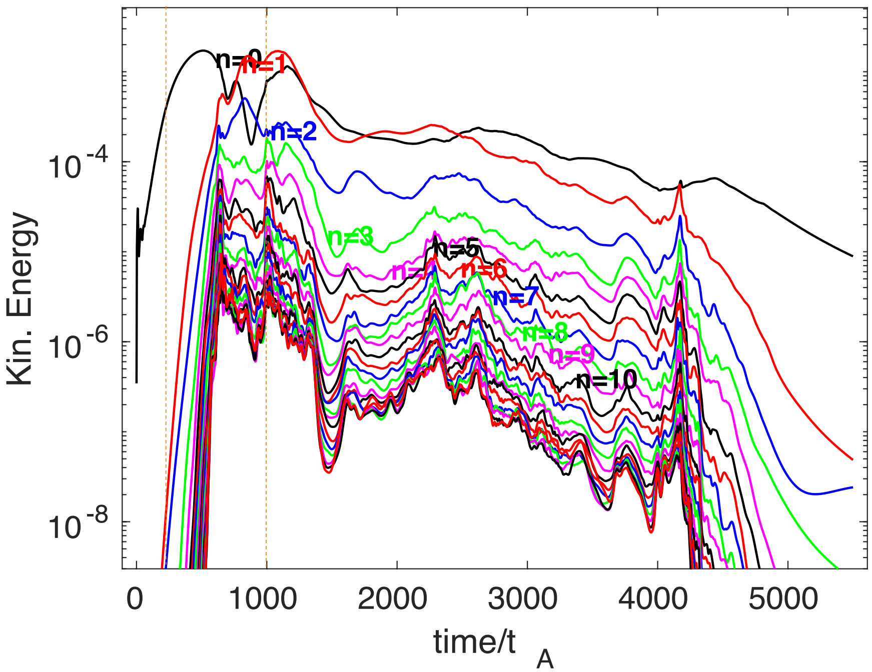

Kinetic energy fluctuations (0≤n≤21) indicate multiple events over time.

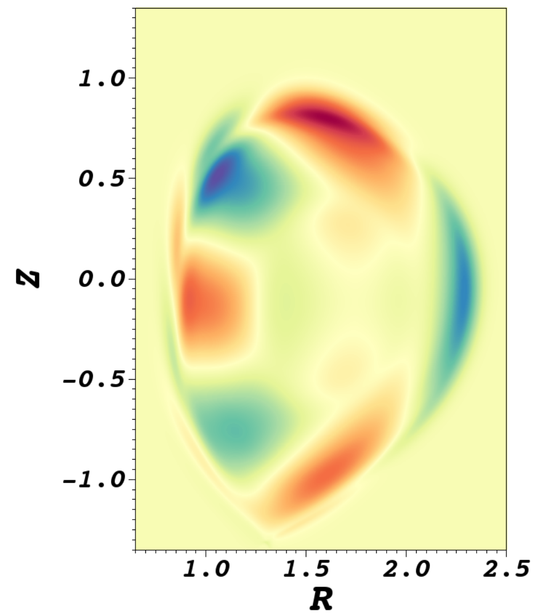

At t = 225, n = 1 pressure contours primarily show m = 3.

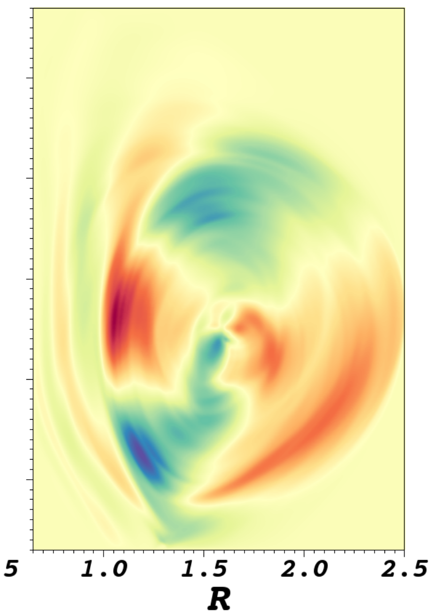

At t = 999, n = 1 perturbations are primarily m = 2.

Global diagnostics show that plasma current persists longer, and energy confinement shorter, with asymmetry.

- The strong m = 2, n = 1 activity shown previously is at the start of the thermal quench.

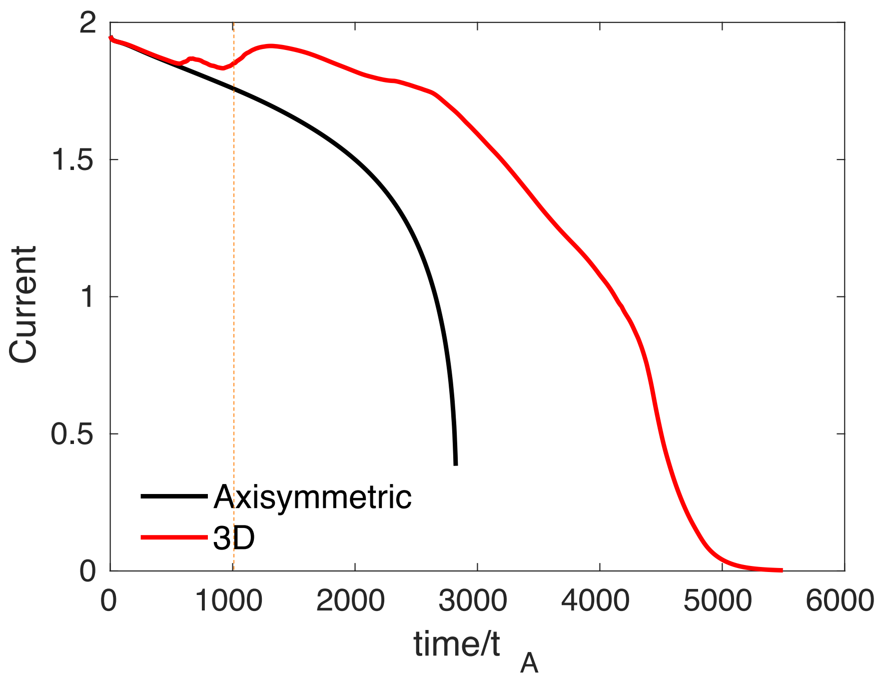

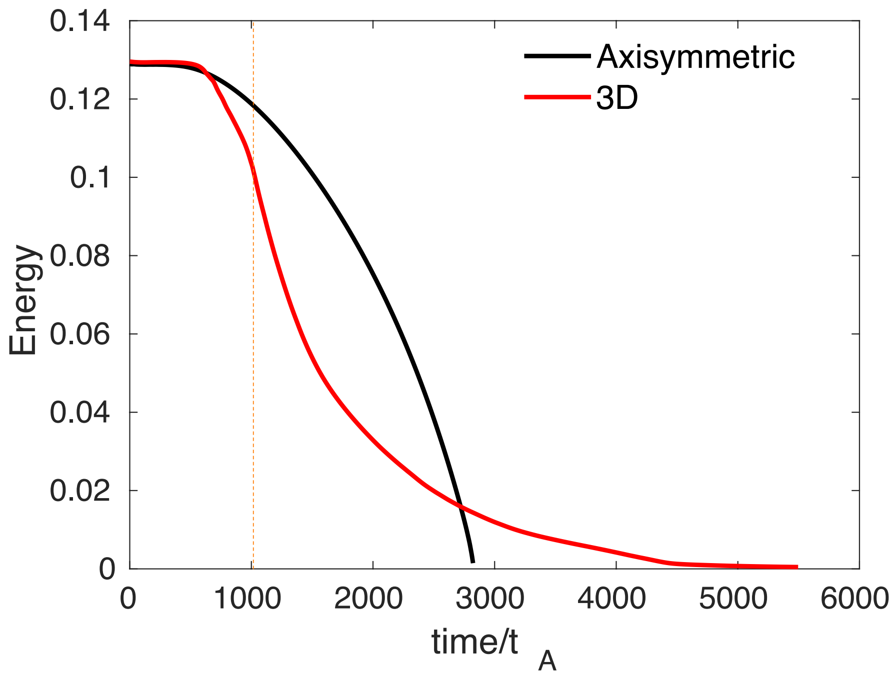

The current in the 3D computation spikes above the 2D result during the peak *n* = 1 activity.

Thermal quenching is faster than the current quench for the 3D case.

As the dominant mode changes from m = 3 to m = 2, loss of flux surfaces initiates the thermal quench.

- Results shown here are from a closely related $0 \le n \le 21$ computation.

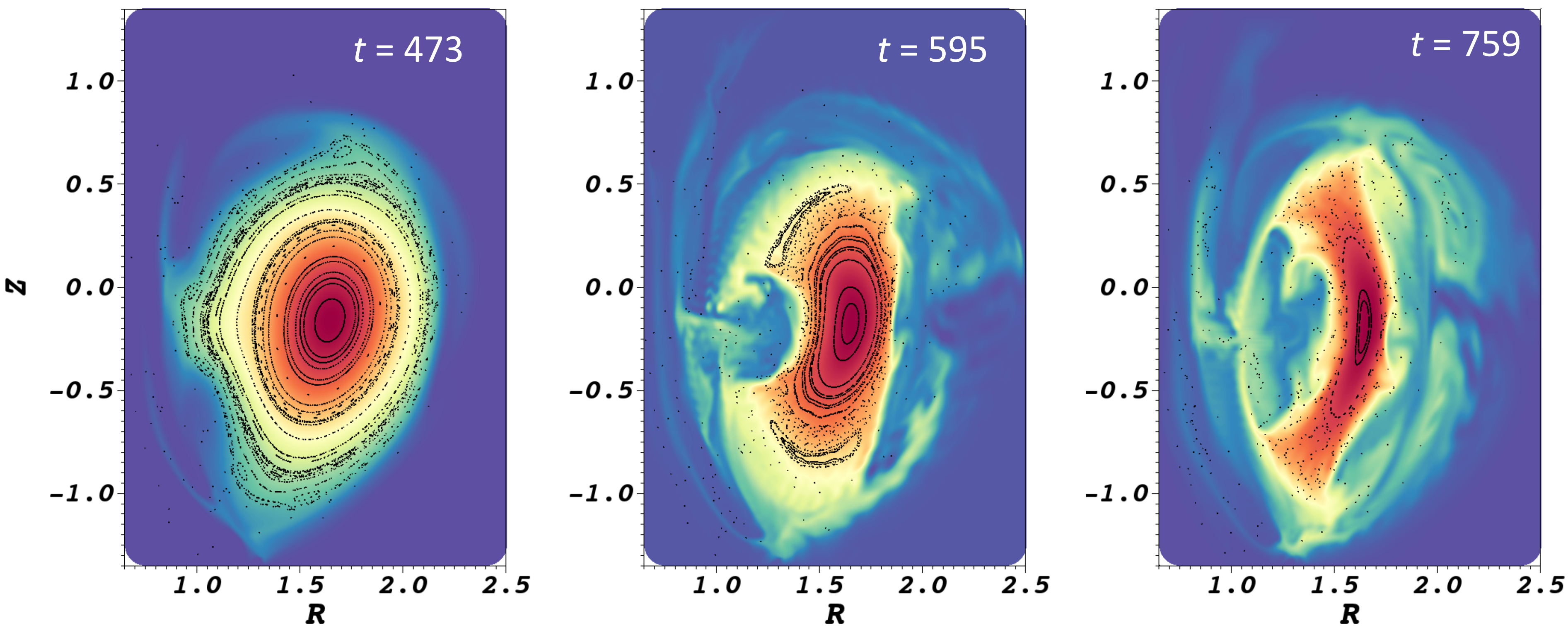

- Poincaré surfaces of section overlaid on pressure show the topology changes that lead to energy loss.

Current spike: Spreading of current density that increases I_p can be described as a dynamo effect.

- The current density profile, $\langle J_{||}/B \rangle$ shown at right, broadens when I_p increases, whereas the flux distribution is relatively unchanged.

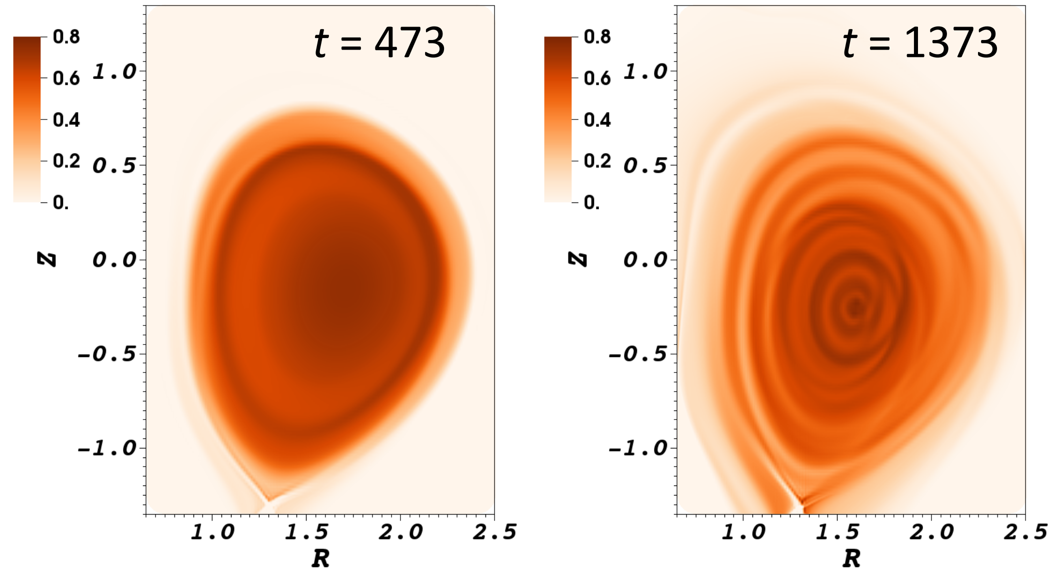

- Correlated fluctuations of flow velocity and magnetic field induce changes in spatially averaged **B**.
  - Averaged Faraday's law with resistive-MHD **E**:

$$\frac{\partial}{\partial t}\langle \mathbf{B} \rangle = -\nabla \times \left[\langle \eta \mathbf{J} \rangle - \langle \mathbf{V} \rangle \times \langle \mathbf{B} \rangle + \langle \mathbf{E}_f \rangle \right]$$

  - MHD dynamo effect from astrophysics, RFP, and spheromak literature is $\langle \mathbf{E}_f \rangle = -\langle \tilde{\mathbf{v}} \times \tilde{\mathbf{b}} \rangle$.

dI_p/dt becomes positive when power transferred by $\mathbf{E}_f$ becomes significant.

- Low-frequency Poynting theorem for $\langle \mathbf{B} \rangle^2$ evolution is

$$\frac{\partial}{\partial t}\frac{\langle \mathbf{B} \rangle^2}{2\mu_0} + \frac{1}{\mu_0}\langle \mathbf{E} \rangle \times \langle \mathbf{B} \rangle = -\langle \mathbf{E} \rangle \cdot \langle \mathbf{J} \rangle$$

- Right side includes fluctuation-induced $-\langle \mathbf{E}_f \rangle \cdot \langle \mathbf{J} \rangle$.

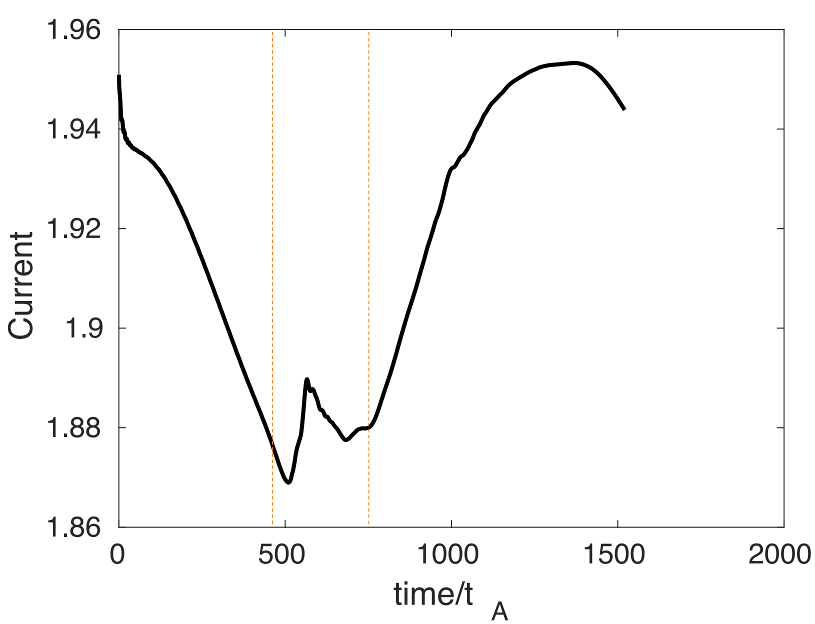

Plasma current spike occurs when *m*=2 becomes dominant.

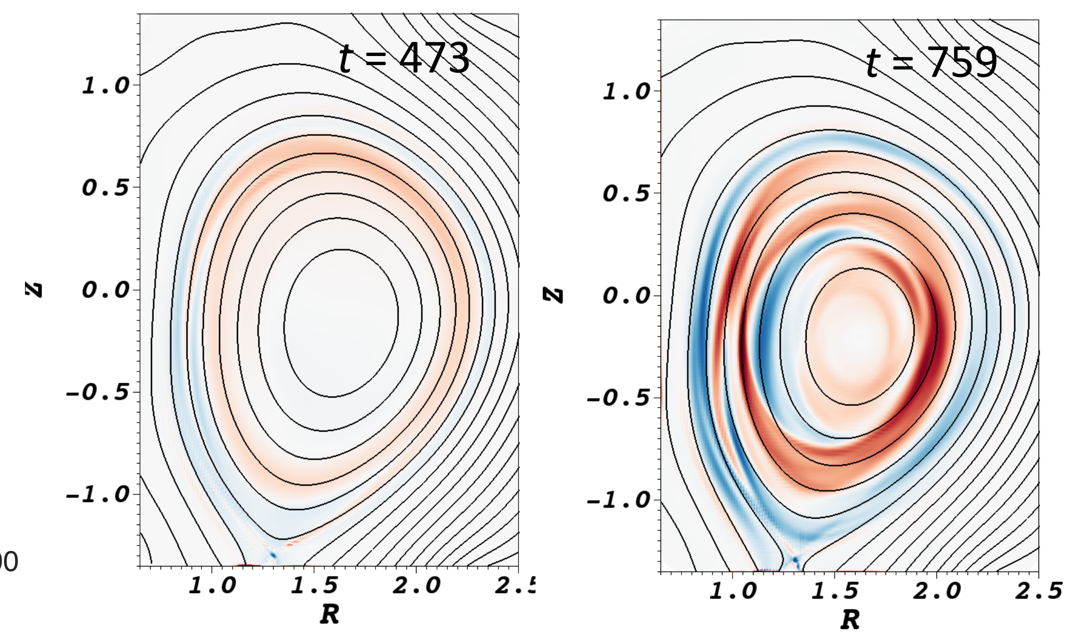

Blue contours show $\langle E_f \rangle . \langle J \rangle$ <0, red is >0, overlaid with poloidal flux contours.

“Relaxation” of parallel current density is not as uniform as it appears in plots of averaged field.

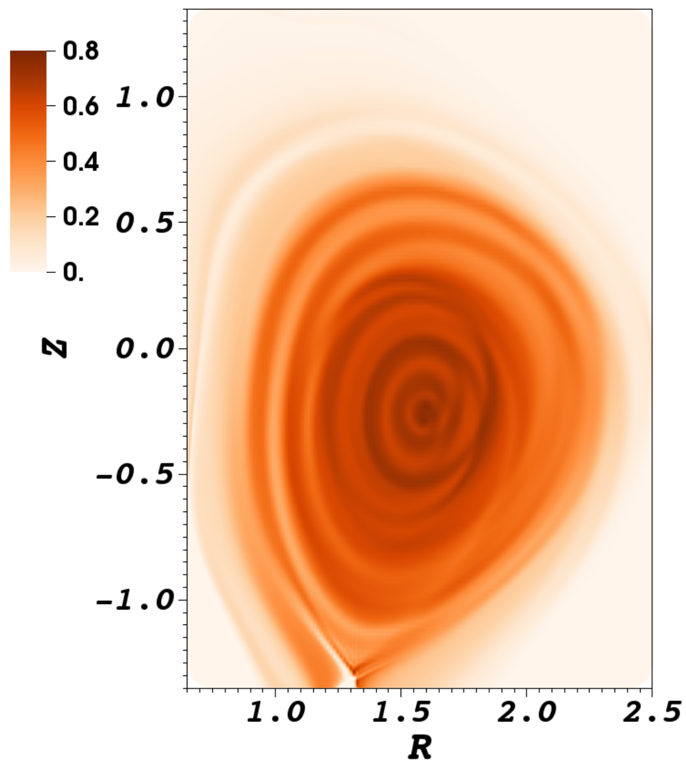

Plot of $\langle \mu_0 J_{||}/B \rangle$ at t = 1373 τ_A of the new simulation, where < > indicates toroidal average.

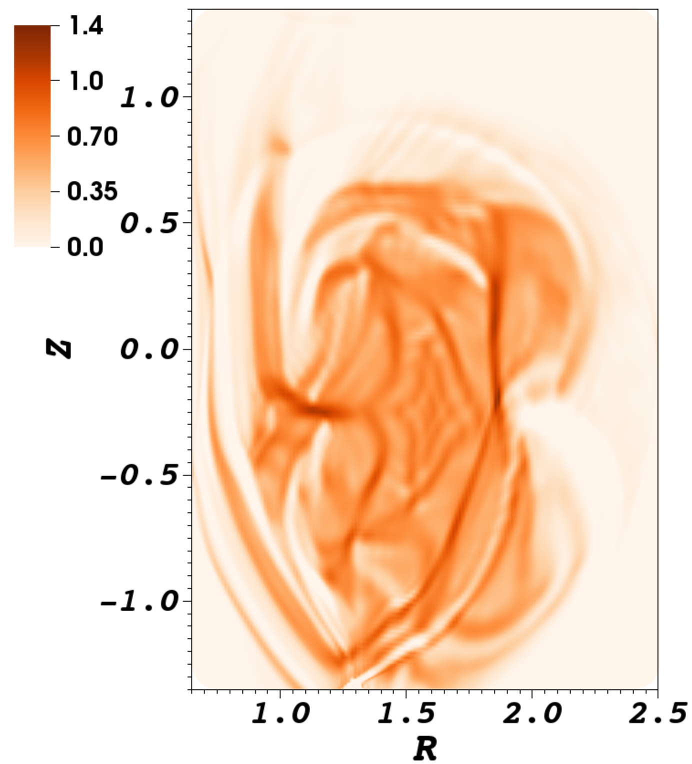

Plot of $\mu_0 J_{||}/B$ over one poloidal slice t = 1373 τ_A.

Wall forces: Forces with a thin-wall model should be computed from stress on outer surface.

- Pustovitov's computation [Nucl. Fusion **55**, 113032] is the natural one to apply with thin-wall modeling.
  - It assumes that the wall and plasma form an electrically isolated system.
  - Plasma inertial force is negligible on τ_{wall} timescale.
- Cartesian components of Lorentz force over any object are $F_j = \hat{\mathbf{e}}_j \cdot \int \mathbf{J} \times \mathbf{B}\, dVol$.
  - With a thin wall, $\mathbf{J}\Delta x \to \mathbf{K}$ as $|\mathbf{J}| \to \infty$, but

    $F_j = \mu_0^{-1} \oint d\mathbf{S} \cdot \left[\mathbf{BB} - \underline{\underline{\mathbf{I}}} B^2/2 \right] \cdot \hat{\mathbf{e}}_j$ holds.
  - Split into integrals over inner and outer surfaces of the wall:

    $$F_{in_j} = \mu_0^{-1} \int_{S_{in}} d\mathbf{S} \cdot \left[\mathbf{BB} - \underline{\underline{\mathbf{I}}} B^2/2 \right] \cdot \hat{\mathbf{e}}_j \, ; \quad F_{out_j} = \mu_0^{-1} \int_{S_{out}} d\mathbf{S} \cdot \left[\mathbf{BB} - \underline{\underline{\mathbf{I}}} B^2/2 \right] \cdot \hat{\mathbf{e}}_j$$
  - Also, $-F_{in}$ acts on plasma, hence $F_{in} \to 0$ for negligible plasma inertia.

    $F_j \to F_{out_j}$

Our computations are consistent with Pustovitov's inferences.

- We compute both F_{out} and F_{in} for the 3D computations.
- Computed results have $F_{in_j} \sim \frac{1}{100} F_{out_j}$.

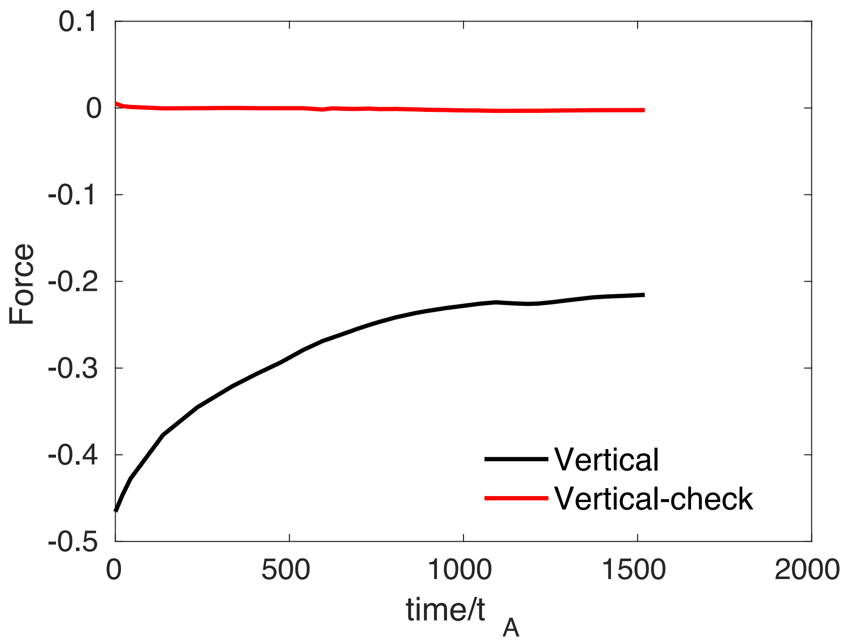

Net forces in vertical direction: F_{out} in black and F_{in} in red.

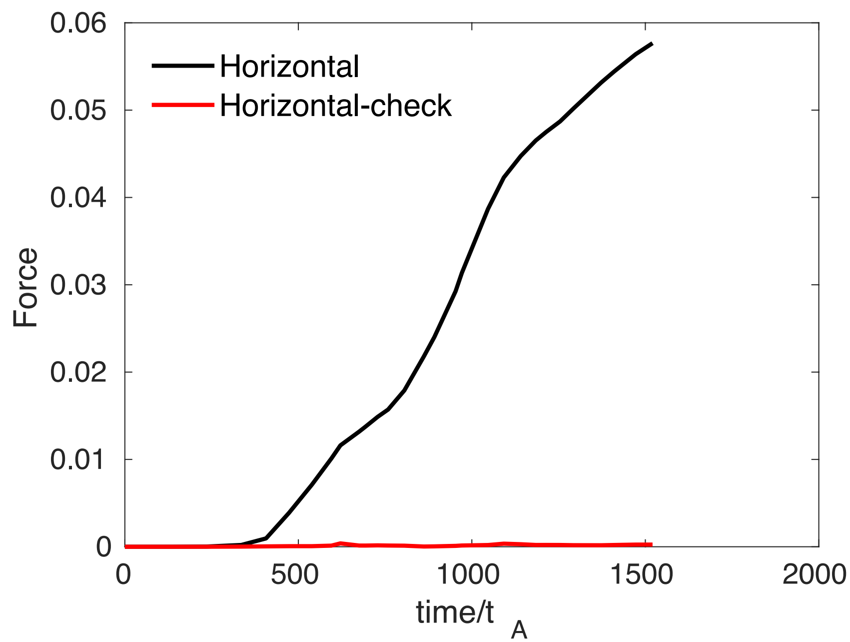

Net horizontal forces: F_{out} in black and F_{in} in red.

Boundary modeling: We are developing more realistic modeling by considering magnetized sheath effects.

- The boundary conditions derived for reduced turbulence modeling in [Loizu, *et al.*, Phys Plasmas **19**, 122307 (2012)] are based on conditions at the magnetic pre-sheath entrance.
- We are adapting these conditions for full-MHD and two-fluid computations.
    - Parallel flow is the ion acoustic speed (at $T_i = 0$)
    - ✧ Electrons are thermally insulated by the sheath (2-*T* modeling is used)
    - Tangential flow is from drifts, including sheath-**E**
    - Wall electrical potential varies along the surface
    - Parallel current is limited by what can be drawn (either ions or electrons, depending on potential drop across sheath)

Magnetic presheath boundary conditions for flow, particle density and temperatures have been implemented.

- Comparison of vertical component of flow from three nonlinear axisymmetric VDE computations indicates the importance of boundary conditions [Bunkers' poster, Tuesday].

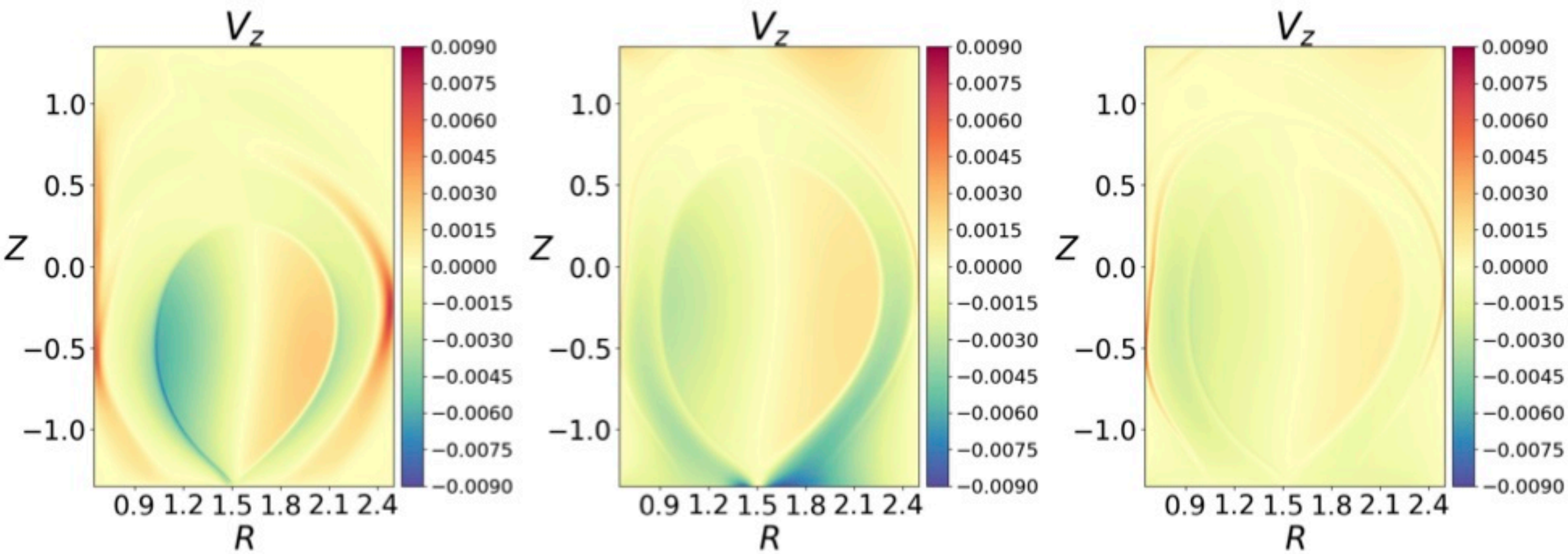

Single-*T* computation with fixed T_{wall} and no normal flow.

Single-*T* computation with Bohm-Chodura outflow and fixed T_{wall}.

Two-*T* computation with Bohm-Chodura outflow and insulated T_e.

- Saturation-current limits on **J** and tangential-**V** conditions are needed to complete the 0^{th}-order model.

Conclusions & Discussion

- Visco-resistive MHD-based computations with NIMROD reproduce important qualitative features:
  - Relatively fast thermal quench
  - Current spike and relatively slow decay (absent RE modeling)
- Spike occurs after TQ has begun, and dynamo effect is relevant.
- Wall-force check supports Pustovitov's approach.

➢ Large 3D MHD computations of disruption are computationally intensive.

  ➢ Improve algorithms and use of hardware.

➢ What reduced runaway model is best for practical CQ computation?

Our computations use visco-resistive (full) MHD with fluid closures.

- The following system is our base non-ideal single-fluid model.

$\frac{\partial n}{\partial t} + \nabla \cdot (n\mathbf{V}) = \nabla \cdot \left(D_n \nabla n - D_h \nabla \nabla^2 n \right)$	particle continuity with artificial diffusion
$mn\left(\frac{\partial}{\partial t} + \mathbf{V} \cdot \nabla \right)\mathbf{V} = \mathbf{J} \times \mathbf{B} - \nabla(2nT) - \nabla \cdot \underline{\Pi}$	momentum density
$\frac{n}{\gamma - 1}\left(\frac{\partial}{\partial t} T + \mathbf{V} \cdot \nabla T \right) = -nT\nabla \cdot \mathbf{V} - \nabla \cdot \mathbf{q}$	temperature evolution
$\frac{\partial \mathbf{B}}{\partial t} = -\nabla \times (\eta \mathbf{J} - \mathbf{V} \times \mathbf{B})$	Faraday's law & resistive MHD Ohm's
$\mu_0 \mathbf{J} = \nabla \times \mathbf{B}$	Ampere's law
$\nabla \cdot \mathbf{B} = 0$	divergence constraint

- The NIMROD code (https://nimrodteam.org) is used to solve linear and nonlinear versions of this system.

Closure relations approximate plasma transport effects.

- Magnetic diffusivity depends on temperature.
  - $\eta(T) = \min\left[\eta_0 \left(T_0/T\right)^{3/2} , 1\right]$
  - $\tau_A/\tau_\eta = \eta_0 \tau_A / \mu_0 a^2 \cong 1\times 10^{-6}$
- Thermal conduction and viscous stress are anisotropic with fixed coefficients.
  - $\mathbf{q} = -n\left[\left(\chi_{\|} - \chi_{iso}\right)\hat{\mathbf{b}}\hat{\mathbf{b}} + \chi_{iso}\underline{\mathbf{I}}\right]\cdot\nabla T\,;\qquad \chi_{\|} = 0.075,\quad \chi_{iso} = 7.5\times 10^{-6}$
  - $\underline{\Pi} = \nu_{\|} mn\left(\underline{\mathbf{I}} - 3\hat{\mathbf{b}}\hat{\mathbf{b}}\right)\hat{\mathbf{b}}\cdot\underline{\mathbf{W}}\cdot\hat{\mathbf{b}} - \nu_{iso} mn\underline{\mathbf{W}}\,;\quad \nu_{\|} = 5\times 10^{-2},\quad \nu_{iso} = 5\times 10^{-5}$

    $\underline{\mathbf{W}} = \nabla\mathbf{V} + \nabla\mathbf{V}^T - \frac{2}{3}\underline{\mathbf{I}}\nabla\cdot\mathbf{V}$
- Artificial particle diffusivities are intended to be small.
  - $D_n = 5\times 10^{-6}\,,\quad D_h = 1\times 10^{-10}$
- NOTE: the equations used in this application have been normalized.
  - $\tau_A \equiv R_0^2 / F_{open} \cong 1;\quad \mu_0 \to 1,\quad n_0 \to 1$
  - $a \cong 0.8\,;\quad R_0 = 1.6$

We surround the inner plasma-containing sub-domain with a resistive wall and outer vacuum.

- Resistive diffusion through the wall is at an intermediate time-scale between τ_A and τ_η.
  - $v_{wall} = \eta_{wall}/\mu_0 \Delta x_{wall} = 1 \times 10^{-3}$
  - The outer vacuum region is surrounded by a conducting wall.
  - Small (10^{-7}) magnetic field errors in *n* = 1 and *n* = 2 are applied in nonlinear 3D computations.

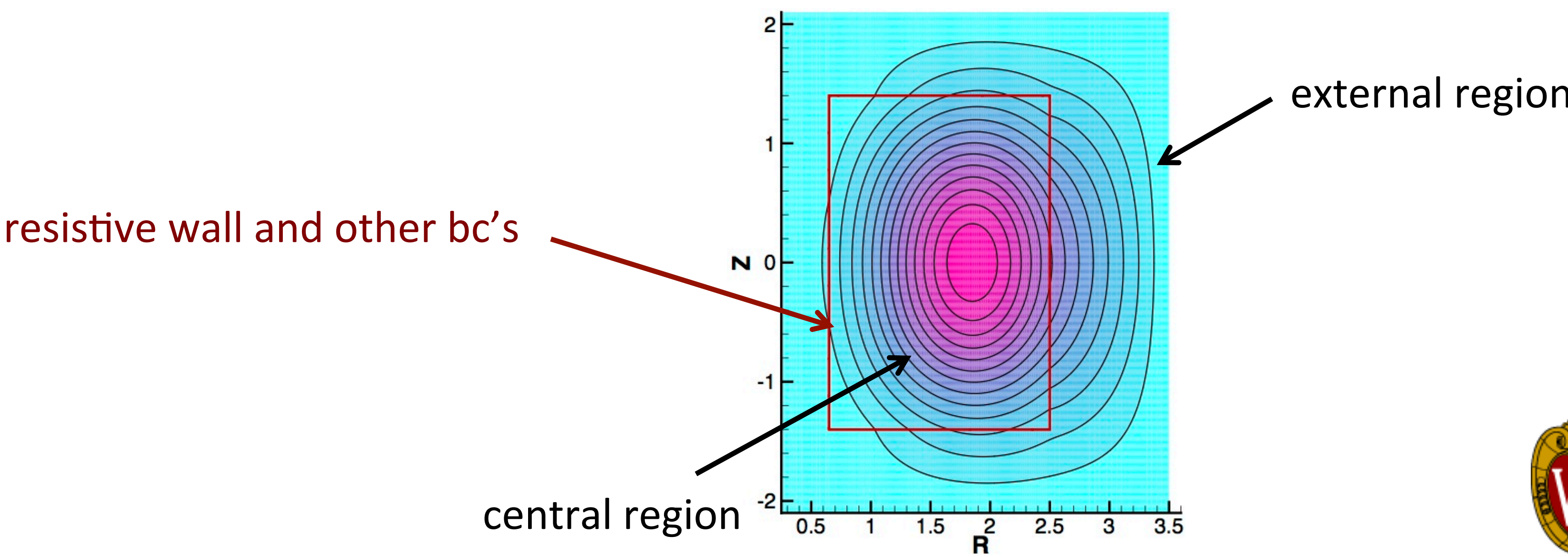

Robust asymmetric instability is a consequence of edge profile changes from wall contact.

- Edge profile changes are most evident from the axisymmetric computation.
- Loss of edge RB_ϕ and pressure enhances edge current.

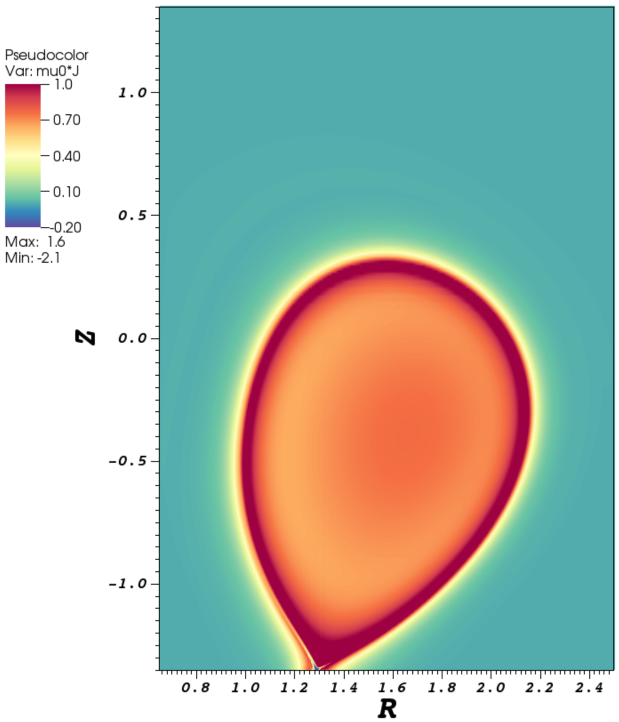

A strong current layer develops at the edge of the closed flux. [Plot shows $<\lambda>=<\mu_0 J_{||}/B>$ at t = 969.]

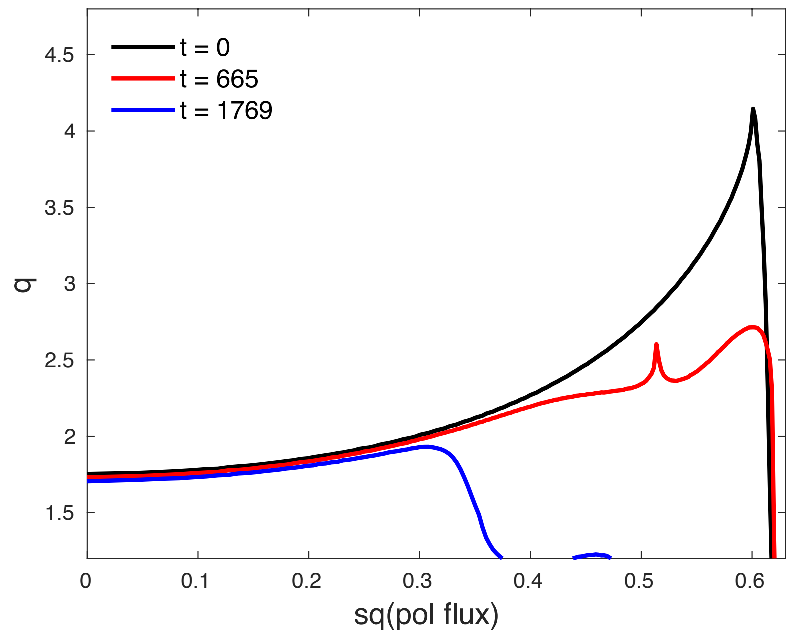

With increasing displacement, edge *q* is reduced.

Evolution of energy fluctuations in long-time and newer simulations are consistent through early phase.

- Evolution of symmetric component of kinetic energy differs significantly, however.

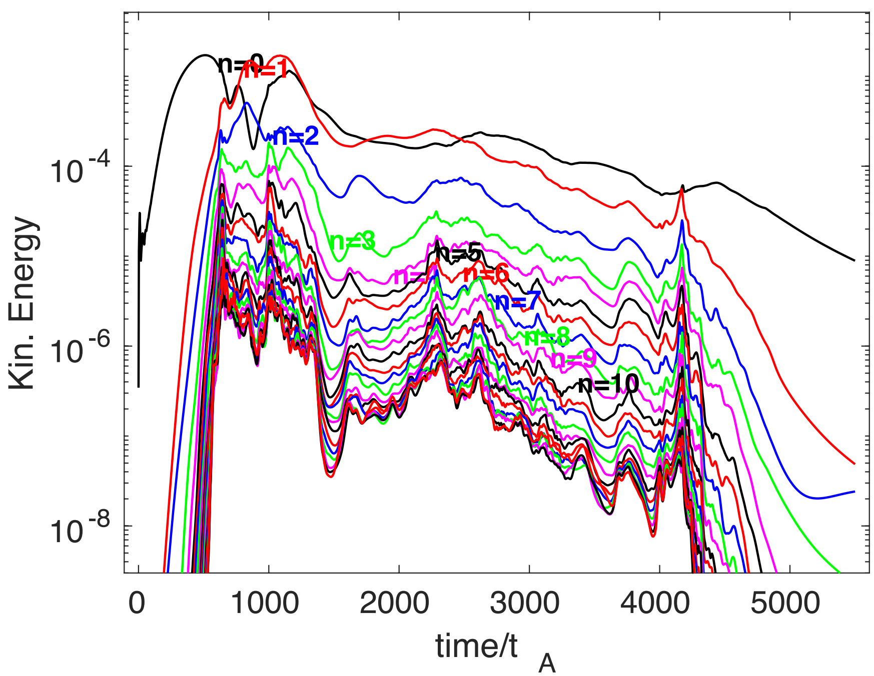

Kinetic energy fluctuations from long-time computation.

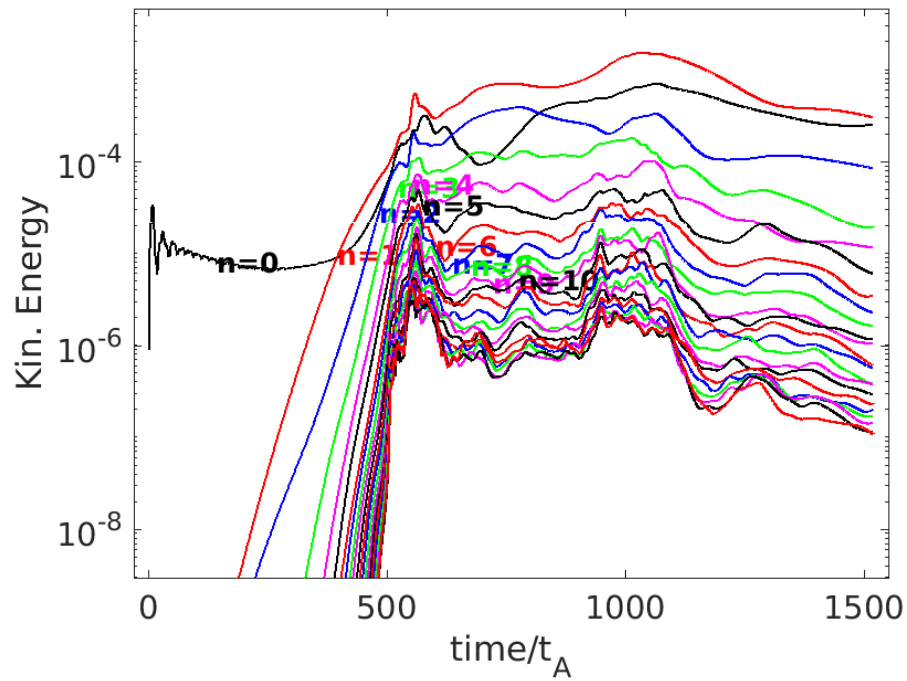

Kinetic energy fluctuations from newer computation.

Horizontal forcing in the 3D computation run to current termination peaks when current decay rate increases.

- Plasma does not support net force, and plasma+wall is an electrically isolated system [Pustovitov, Nucl Fusion **55**, 113032].
- Computation of $F_j = \mu_0^{-1} \oint d\mathbf{S} \cdot \left[\mathbf{BB} - \underline{\underline{\mathbf{I}}} B^2/2 \right] \cdot \hat{\mathbf{e}}_j$ is over the outside of the resistive wall.

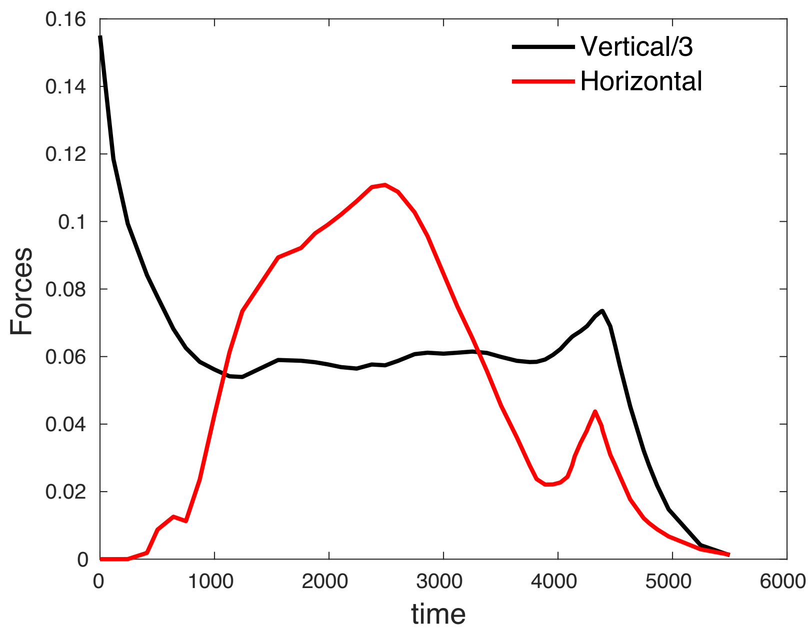

Net horizontal forcing results from vertical I_p excursions crossing B_ϕ, supported by the wall.

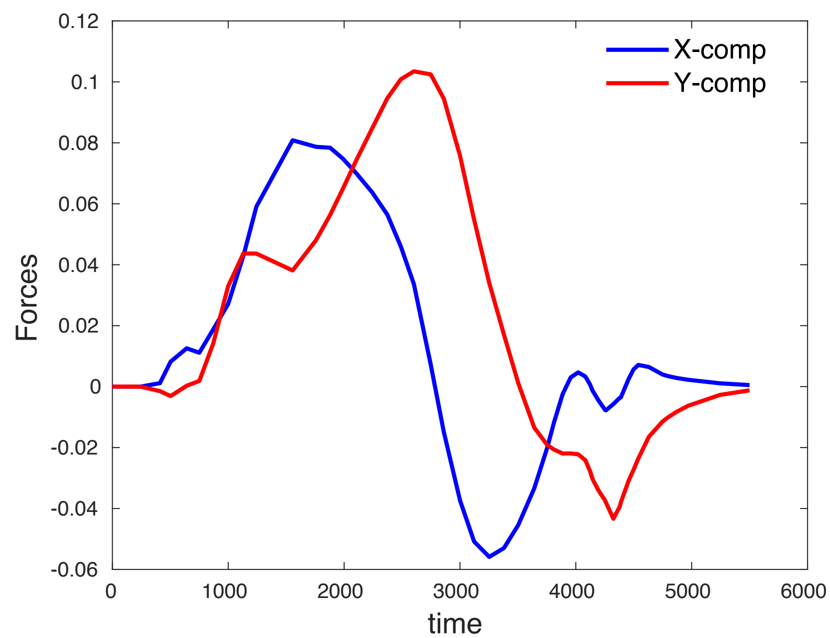

Cartesian components in the horizontal plane indicate slow rotation of the force.